

Lyman- α emission properties of simulated galaxies: interstellar medium structure and inclination effects

Anne Verhamme^{1,2}, Yohan Dubois^{1,3}, Jeremy Blaizot², Thibault Garel^{2,4}, Roland Bacon², Julien Devriendt^{1,2}, Bruno Guiderdoni², Adrienne Slyz¹

¹ Oxford Astrophysics, University of Oxford, Denys Wilkinson Building, Keble Road, Oxford, OX1 3RH, UK.

² Université de Lyon, Lyon, F-69003, France ;

Université Lyon 1, Observatoire de Lyon, 9 avenue Charles André, Saint-Genis Laval, F-69230, France ;

CNRS, UMR 5574, Centre de Recherche Astrophysique de Lyon ;

Ecole Normale Supérieure de Lyon, Lyon, F-69007, France.

³ Institut d'Astrophysique de Paris, 98 bis boulevard Arago, 75014 Paris, France.

⁴ Centre for Astrophysics & Supercomputing, Swinburne University of Technology, P.O. Box 218, Hawthorn, VIC 3122, Australia.

Received date / Accepted date

Abstract

Aims. This paper is the first of a series investigating Lyman-alpha (hereafter Ly α) radiation transfer through hydrodynamical simulations of galaxy formation. Its aim is to assess the impact of the interstellar medium (ISM) physics on Ly α radiation transfer and to quantify how galaxy orientation with respect to the line of sight alters observational signatures.

Methods. We compare the results of Ly α radiation transfer calculations through the ISM of a couple of idealized galaxy simulations in a dark matter halo of $\sim 10^{10} M_{\odot}$. In the first one, G1, this ISM is modeled using physics typical of large scale cosmological hydrodynamics simulations of galaxy formation, where gas is prevented from radiatively cooling below 10^4 K. In the second one, G2, gas is allowed to radiate away more of its internal energy via metal lines and consequently fragments into dense star-forming clouds.

Results. First, as expected, *the small-scale structuration of the ISM plays a determinant role in shaping a galaxy's Ly α properties.* The artificially warm, and hence smooth, ISM of G1 yields an escape fraction of $\sim 50\%$ at the Ly α line center, and produces symmetrical double-peak profiles. On the contrary, in G2, most young stars are embedded in thick star-forming clouds, and the result is a ~ 10 times lower escape fraction. G2 also displays a stronger outflowing velocity field, which favors the escape of red-shifted photons, resulting in an asymmetric Ly α line. Second, *the Ly α properties of G2 strongly depend on the inclination at which it is observed:* From edge-on to face-on, the line goes from a double-peak profile with an equivalent width of $\sim -5\text{\AA}$ to a 15 times more luminous red-shifted asymmetric line with EW $\sim 90\text{\AA}$.

Conclusions. The remarkable discrepancy in the Ly α properties we derived for two ISM models raises a fundamental issue. In effect, it demonstrates that Ly α radiation transfer calculations can only lead to realistic properties in simulations where galaxies are resolved into giant molecular clouds. Such a stringent requirement translates into severe constraints both in terms of ISM physics modeling and numerical resolution, putting these calculations out of reach of current large scale cosmological simulations. Finally, we find inclination effects to be much stronger for Ly α photons than for continuum radiation. This could potentially introduce severe biases in the selection function of narrow-band Ly α emitter surveys, and in their interpretation, and we predict these surveys could indeed miss a significant fraction of the high- z galaxy population.

Key words. Radiative transfer – Hydrodynamics – ISM: structure, kinematics and dynamics – Galaxies: formation, ISM

1. Introduction

In the last decade, the Lyman-alpha (Ly α) emission line has become an observational tool of choice to detect high redshift galaxies via narrow-band surveys (e.g. Hu et al. 1998; Kudritzki et al. 2000; Shimasaku et al. 2006; Ouchi et al. 2008, 2010; Hu et al. 2010) or blind spectroscopic searches (e.g. van Breukelen et al. 2005; Rauch et al. 2008; Cassata et al. 2011). Today, the number of galaxies detected in this fashion (hereafter Lyman-Alpha Emitters, LAE) is becoming statistically significant, and LAEs play a major role in our census of high- z galaxies. At the same time, spectroscopic follow-ups of UV-selected galaxies shed more and more light on the physical nature of LAE and on their place in the cosmic history of galaxy formation (Shapley et al. 2003; Tapken et al. 2007; Bielby et al. 2011). One of the major challenges in the years to come, both theoretical and ob-

servational, is yet to understand the details of the Ly α line profiles we observe: How do they relate (if they do) to any physical property of high- z galaxies ?

Although a number of semi-analytic models for Lyman-alpha Emitting galaxies (LAEs) have been published (e.g. Le Delliou et al. 2006; Orsi et al. 2008; Dayal et al. 2008, 2009; Orsi et al. 2011; Dayal et al. 2011; Garel et al. 2012), the complete radiation transfer through *the interstellar medium* of Ly α emitting galaxies has been taken into account in only a handful of previous studies (Tasitsiomi 2006; Laursen et al. 2009; Barnes et al. 2011; Yajima et al. 2011a,b, see Table 1 for a summary.).

In Tasitsiomi (2006), Ly α radiation transfer is post-processed in the brightest Ly α emitter of a gas-dynamics+N-body adaptive refinement tree (ART, Kravtsov and Gnedin 2005) simulation at $z \sim 8$, in order to investigate its detectability. In Laursen et al. (2009), a sample of nine galaxies at $z = 3.6$ taken from cosmological N-body/hydrodynamical TreeSPH simula-

Send offprint requests to: anne.verhamme@univ-lyon1.fr

	this study	Tasitsiomi (2006)	Laursen et al. (2009)	Barnes et al. (2011)	Yajima et al. (2011a,b)
context	Ly α emitting galaxies	Ly α emitting galaxies	Ly α emitting galaxies	DLA-host galaxies	Ly α emitting galaxies
hydro technics	AMR (RAMSES)	AMR (ART)	SPH (TreeSPH)	SPH (GADGET)	SPH (GADGET)
Ly α RT	Ly α + continuum AMR	Ly α , no dust AMR	Ly α AMR	Ly α , no dust cartesian	Ly α + continuum AMR
Ly α sources	recombination from young stars	recombination from young stars	recombination + gravitational cooling + UV background	central point source	recombination + collisional excitation
environment	isolated galaxy	cosmo zoom	cosmo zoom	cosmo zoom	cosmo zoom
nb of objects	2	1	9	3	~ 950
stellar mass	$1.8 \times 10^9 M_{\odot}$ for G1 $4.9 \times 10^8 M_{\odot}$ for G2	$\sim 10^{10} M_{\odot}$	6×10^6 to $3 \times 10^{10} M_{\odot}$	$1.5 \times 10^{10} M_{\odot}$ $1.5 \times 10^{11} M_{\odot}$ $7.5 \times 10^{11} M_{\odot}$	$4.3 \times 10^9 M_{\odot}$ $9.3 \times 10^9 M_{\odot}$ $4.1 \times 10^{10} M_{\odot}$
stellar mass resolution	$1.4 \times 10^3 M_{\odot}$ for G2 $7.7 \times 10^3 M_{\odot}$ for G1	$2 \times 10^4 M_{\odot}$	$10^6 M_{\odot}$	not available	$1.9 \times 10^4 M_{\odot}$
spatial resolution ^(a)	18 pc for G2 147 pc for G1	29 pc	137 pc ^(b)	514 pc	342 pc
H I temperature	10^2 to 10^5 K	10^3 to 10^4 K	10^4 K	$10^{4.3}$ to 10^5 K	-

Table 1. Comparison of the 4 published studies of Ly α radiation transfer through the interstellar medium of galaxies with this study.

^(a) Resolution, in physical pc . This is either the minimum cell size, for AMR codes, or the gas gravitational softening length for SPH codes. In both cases, this reflects the smallest scale onto which a gas overdensity may feel its own gravity.

^(b) This resolution corresponds to their S87 simulation, which best matches our halo mass.

tions (Sommer-Larsen 2006) are considered, sampled in mass. The main result of the paper is an anti-correlation between Ly α escape fraction and the mass of the galaxy. In Barnes et al. (2011), three halos at $z = 3$ are selected in cosmological hydrodynamic simulations (GADGET-2) aimed at reproducing the physical properties of the host galaxies of DLAs at $z \sim 3$ (Tescari et al. 2009). In Yajima et al. (2011a,b), the same halo is followed at different redshifts, in order to study the evolution of the Ly α properties of their galaxies with time.

These previous studies are done through a warm interstellar medium in which the gas is cooled down to $T \sim 10^4$ K, with the consequence that the formation of small scale structures is not modelled. Indeed, the pressure support of this warm gas prevents it from collapsing at scales smaller than its Jeans length, explaining the difference in spatial resolution between the different experiments (see section 2 for more details). However, theoretical expectations suggest a strong dependance of the Ly α transfer on the structure, and geometry of the interstellar medium of galaxies, and the main goal of our study is to investigate this point. Furthermore, two studies are dust-free, which prevent them from studying the Ly α escape fraction from their configurations. Finally, monochromatic approaches of the problem do not allow to derive Ly α equivalent widths, and compare the transfer of continuum versus line photons.

To overcome these limitations, we post-process hydrodynamical simulations of galaxy formation described in Dubois and Teyssier (2008) performed with the RAMSES code (Teyssier 2002), with McLya (Verhamme et al. 2006), including Ly α +continuum radiation transfer in a dusty medium, for two different ISM models : 1/ the reference model G1, comparable to previous studies, where the gas is cooled down to 10^4 K, 2/ a more realistic ISM model G2, where the gas is allowed to cool down to 100K, and the formation of small scale structures is followed.

The plan of this paper is the following. We start to describe the hydrodynamical simulations used to post-process Ly α radiation transfer. Then, we describe the radiative transfer of Ly α photons in the hydrodynamical simulations with McLya. The fourth part presents a comparison of the Ly α properties for the two ISM models. In the fifth part, we discuss the effect of ori-

entation on the Ly α properties of G2, which appears as an interesting bonus result of this work. The sixth part describes the diffuse Ly α halo around G2. The last part summarizes the main conclusions.

2. Description of the hydrodynamical simulations

The results presented in this paper are based on the analysis of a couple of idealized high-resolution hydrodynamical simulations which follow the formation and evolution of an isolated disc galaxy embedded in a live dark matter (DM) halo. Both simulations were run with RAMSES (Teyssier 2002), using sub-grid physics modules described in Rasera and Teyssier (2006) and Dubois and Teyssier (2008).

2.1. Initial Conditions

We choose to follow the formation of a galaxy embedded in a halo of total mass (dark matter plus gas) $M_{200} = 10^{10} M_{\odot}$. The choice of this rather small halo mass is motivated by the expectation that most small-mass haloes host LAEs, while only a fraction of massive galaxies emit Lyman-alpha at all (see e.g. Garel et al. 2012, and references therein).

We assume a NFW density profile (Navarro et al. 1996) with concentration parameter $c = 10$ for the DM halo. The ‘virial’ radius $R_{200} \sim 35$ kpc of this latter is defined so that it encloses an average density equal to 200 times the mean matter density of the Universe at $z = 0$, assuming $\Omega_m = 1$ and $h = 1$. Note that with the currently favored cosmology (e.g. Komatsu et al. 2011), this value of R_{200} corresponds to a $z \sim 1$ halo of the same mass.

We follow Dubois and Teyssier (2008) to generate our idealized initial conditions and sample the DM halo with particles instead of using a static gravitational potential. This is necessary to allow gas and stars to exchange angular momentum with the DM. This process is particularly important in simulations where gas fragmentation occurs in the disc because the resulting star forming and gravitationally bound clouds should be driven to the bottom of the potential well by dynamical friction. In practice, we sample our halo out to a radius of $3.2 \times R_{200}$ with 10^5 DM particles of mass $\sim 1.8 \times 10^5 M_{\odot}$.

	G1	G2
Stellar mass M_\star	$2.1 \times 10^9 M_\odot$	$6.8 \times 10^8 M_\odot$
Gas mass M_{gas}	$5.0 \times 10^8 M_\odot$	$3.0 \times 10^8 M_\odot$
M_\star/M_{gas}	~ 4	~ 2
Dust mass M_{dust}	$8.7 \times 10^6 M_\odot$	$6.3 \times 10^6 M_\odot$
SFR	0.3M $_0$ /yr	1.1M $_0$ /yr

Table 2. Comparison of the physical properties of G1 and G2. From the SFR, and assuming a Salpeter IMF, we can derive intrinsic Ly α luminosities of our galaxies: $L(\text{Ly}\alpha)_{\text{G1}} = 3.3 \times 10^{41} \text{erg.s}^{-1}$ and $L(\text{Ly}\alpha)_{\text{G2}} = 1.2 \times 10^{42} \text{erg.s}^{-1}$.

In order to form a centrifugally supported gas disc, we give this distribution of DM particles a specific angular momentum profile $j(r) = j_{\text{max}} \times M(< r)/M_{200}$, where r is the distance to the halo center. The normalization j_{max} is fixed by setting the dimensionless spin parameter of the halo to $\lambda = 0.04$ (see e.g. Bullock et al. 2001). The initial gas density profile is obtained by scaling that of the DM by the universal baryonic fraction $f_b = 0.15$. The gas velocity field is chosen to be identical to that of the DM. We enforce hydrostatic equilibrium, which uniquely defines the gas initial temperature (or pressure) profile, and its chemical composition is pristine (76 % Hydrogen and 24 % Helium in mass).

The simulated volume is a cubic box of size $L_{\text{box}} = 300$ kpc on a side, sufficiently large to self-consistently follow the collapse of the gaseous halo for up to 6 Gyrs. Open boundary conditions let the galactic wind stream out of the box freely. The snapshots are chosen at the time where the galactic wind is reaching the virial radius, i.e. after 3 Gyr for G1 and 1 Gyr for G2. Although ages are different, M_{gas} and M_{dust} are comparable for G1 and G2 (See Table 2). The adaptive mesh refinement (AMR) grid is composed of 64^3 cells on the coarsest level, which corresponds to a cell size of ~ 4.7 kpc. Levels of refinement are triggered when at least one of the two following criteria is fulfilled:

1. The total baryonic mass in a cell becomes larger than $6 \times 10^4 M_\odot$, or a cell contains at least 8 DM particles
2. A cell size becomes larger than $0.25\lambda_J$ (Truelove et al. 1997)

Refinement is allowed up to a maximum level which depends on the simulation. In our G1 (resp. G2) simulation (see Tab. 1 and Sec. 2.2), the maximum level allowed is 11 (resp. 14), which corresponds to a spatial resolution of 147 pc (resp. 18 pc).

2.2. Physics of galaxy formation

In this subsection, we briefly discuss how the physics (besides gravity and hydrodynamics) relevant to galaxy formation is modeled in the simulations. Table 2 summarizes the global properties of G1 and G2.

Cooling: Radiative energy losses, assuming gas is in collisional ionization equilibrium, are computed in each grid cell using the metallicity dependent cooling functions tabulated in Sutherland and Dopita (1993). This allows the gas to cool down to 10^4 K in runs G1 and G2. In G2, we also account for the extra loss of energy provided by metal line cooling, following the prescription of Rosen and Bregman (1995). This allows the temperature of the gas to drop further down, to 100K in this run.

Interstellar Medium: In order to prevent numerical fragmentation, we assume the ideal gas transitions to a polytropic equation

of state (EoS) in high-density regions

$$T = T_0 \left(\frac{\rho}{\rho_0} \right)^{p-1}, \quad (1)$$

where p is the polytropic index, ρ_0 is the gas density above which the polytropic law applies, and T_0 is the minimum temperature of the gas due to cooling. We adopt a $p = 2$ polytropic index that ensures that the Jeans length is independent of the gas density for densities above ρ_0 . For run G1, $T_0 = 10^4$ K and $\rho_0 = 0.1 \text{H.cm}^{-3}$, and the Jeans length of the gas is $\lambda_J \simeq 5.8$ kpc, comparable to the size of the entire galactic disc. This means that the ISM gas does not fragment, but instead is smoothly distributed throughout the disc (see Fig 1). For run G2, $T_0 = 100$ K, and $\rho_0 = 10 \text{H.cm}^{-3}$, so the constant Jeans length given by the polytropic EoS is $\lambda_J = 58$ pc, which we resolve with ~ 3 cells of size $\Delta x = 18$ pc. This choice of T_0 and ρ_0 creates a multiphase medium with cold and dense bounded regions of size ~ 100 pc similar to the large giant molecular clouds (GMCs) of the Milky Way, and a low-density warm medium with strong turbulent motions (see Fig 2).

Star formation: Star formation is modeled as in Rasera and Teyssier (2006), with a random Poisson process spawning star cluster particles according to a classic Schmidt law. In other words, the star formation rate $\dot{\rho}_*$ scales with the local gas density ρ as

$$\dot{\rho}_* = \epsilon_* \frac{\rho}{t_{\text{ff}}}, \quad (2)$$

where t_{ff} is the free fall time and ϵ_* is the star formation efficiency. We adopt $\epsilon_* = 1\%$ in runs G1 and G2, which is in fair agreement with observations over the gas density range we span (Krumholz and Tan 2007). Star formation is only permitted to occur in grid cells where the gas density is larger than ρ_0 . Each star-cluster particle created is given a mass which is an integer multiple of the minimal mass $m_* = \rho_0 \times \Delta x^3$, where Δx is the size of a cell on the highest level of refinement. Therefore, our stellar mass resolution is $m_* \simeq 1.4 \times 10^3 M_\odot$ for the G2 simulation (and $m_* \simeq 7.7 \times 10^3 M_\odot$ for the G1 simulation). We forbid the star formation process to consume more than 90% of the gas mass in the cell where it takes place during a time step.

Feedback: We model supernovae (SN) feedback as in Dubois and Teyssier (2008), i.e. we deposit kinetic energy in a sphere centered on the explosion, along with mass and momentum distributed according to a Sedov-Taylor blast-wave profile. This kinetic approach ensures the formation of large-scale galactic winds in low-mass haloes, and galactic fountains in the most massive ones even at low resolution (Dubois and Teyssier 2008). Such a precaution is necessary since it is well known that spurious thermal energy losses are catastrophic (Navarro and White 1993). We assume a standard Salpeter (1955) Initial Mass Function (IMF), with $\eta_{\text{SN}} = 10\%$ (in mass) of the newly formed stars finishing their ~ 10 Myr lives as type II SN. We further assume that 10^{51} ergs of energy are released by each individual SN explosion with a typical ejected mass of $10 M_\odot$. SN are also responsible for releasing metals into their surroundings with a constant yield $y = 0.1$. These metals are passively advected.

3. Ly α transfer

We use an improved version of the Monte Carlo radiation transfer code McLy α of Verhamme et al. (2006) to post-process the two simulations G1 and G2 described in Sec. 2. The most notable technical improvement over the original McLy α is that it

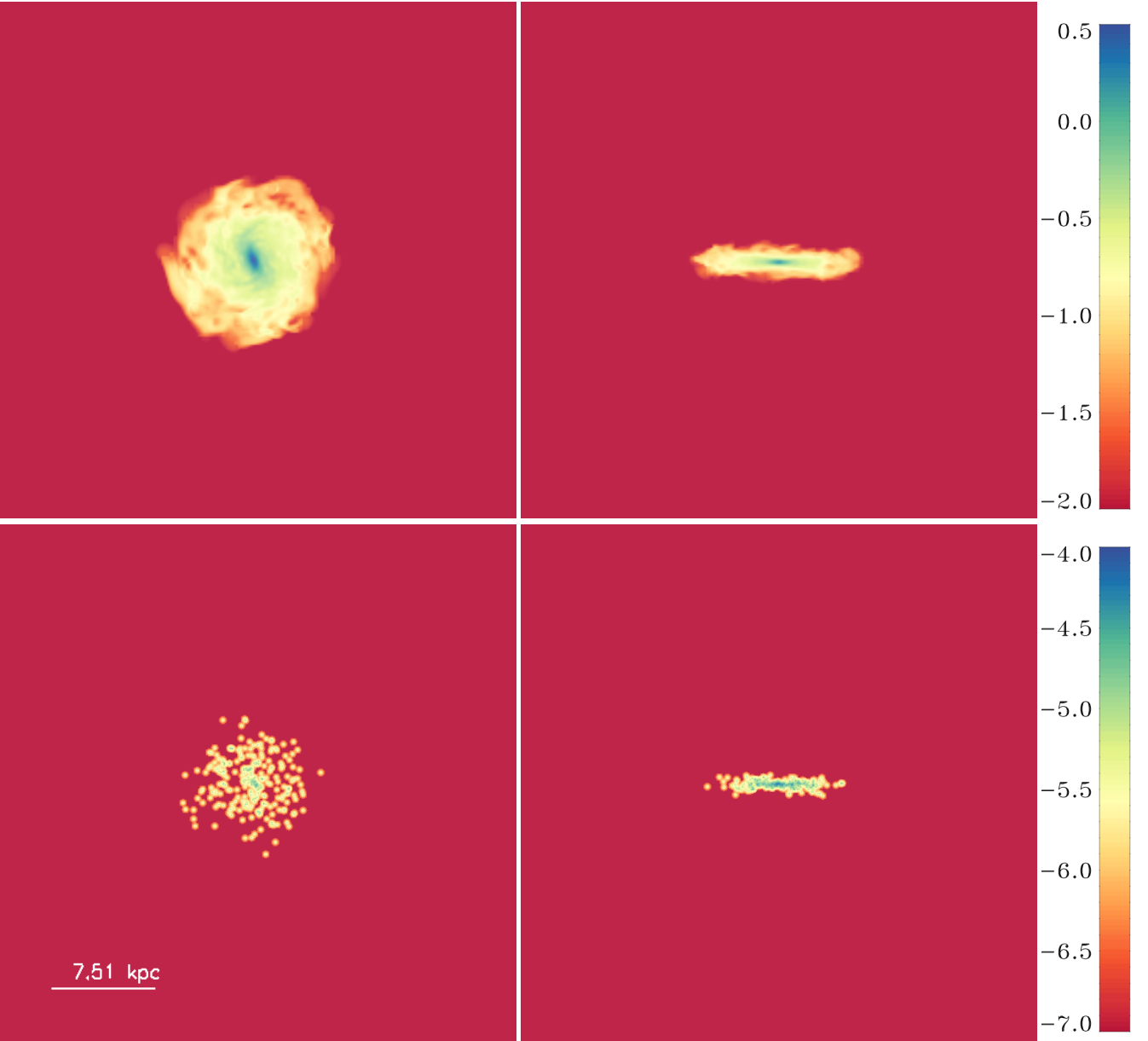


Figure 1. **Left :** G1 run galaxy seen face-on. **Right :** G1 run galaxy seen edge-on. The upper panels show the distribution of the gas density (in $\log \text{cm}^{-3}$ units), and the bottom panels the distribution of stellar density for stars younger than 10 Myr (in arbitrary log units) .

now fully exploits the AMR grid structure of RAMSES, which allows us to perform the radiative transfer at the same spatial resolution than our hydrodynamics simulations. The new version of `McLya` also features more detailed physics of the Ly α line and UV continuum transfer, which include (see Schaerer et al. 2011): angular redistribution functions taking quantum mechanical effects for Ly α into account (Dijkstra and Loeb 2008; Stenflo 1980), frequency changes of Ly α photons due to the recoil effect (e.g. Zheng and Miralda-Escudé 2002), the presence of deuterium (assuming a canonical abundance of $D/H = 3 \times 10^{-5}$, Dijkstra et al. 2006), and anisotropic dust scattering using the Henyey-Greenstein phase function (using parameters adopted in Witt and Gordon 2000).

Before `McLya` can be used to process our simulations, we have to extract a set of gas properties for each cell which are not directly predicted by RAMSES: the gas velocity dispersion

due to temperature and small-scale turbulence (the macroscopic velocity and temperature of each cell are known), the ionization state (or equivalently the neutral Hydrogen density), and the dust content. We discuss how we compute these quantities in the following sub-sections, and then explain our strategy to sample Ly α emission.

3.1. Ionisation state of the gas

The simulation outputs provide us with the total density ρ of gas in each cell, including H, He and metals. We derive the numerical density of H as $n_H = X_H \rho / m_H$, where $X_H = 0.76$ is the mass fraction of H, and m_H the mass of an H atom. Ly α photons however only scatter onto neutral Hydrogen atoms (H I), the numerical density of which we compute as $n_{\text{HI}} = x n_H$, where

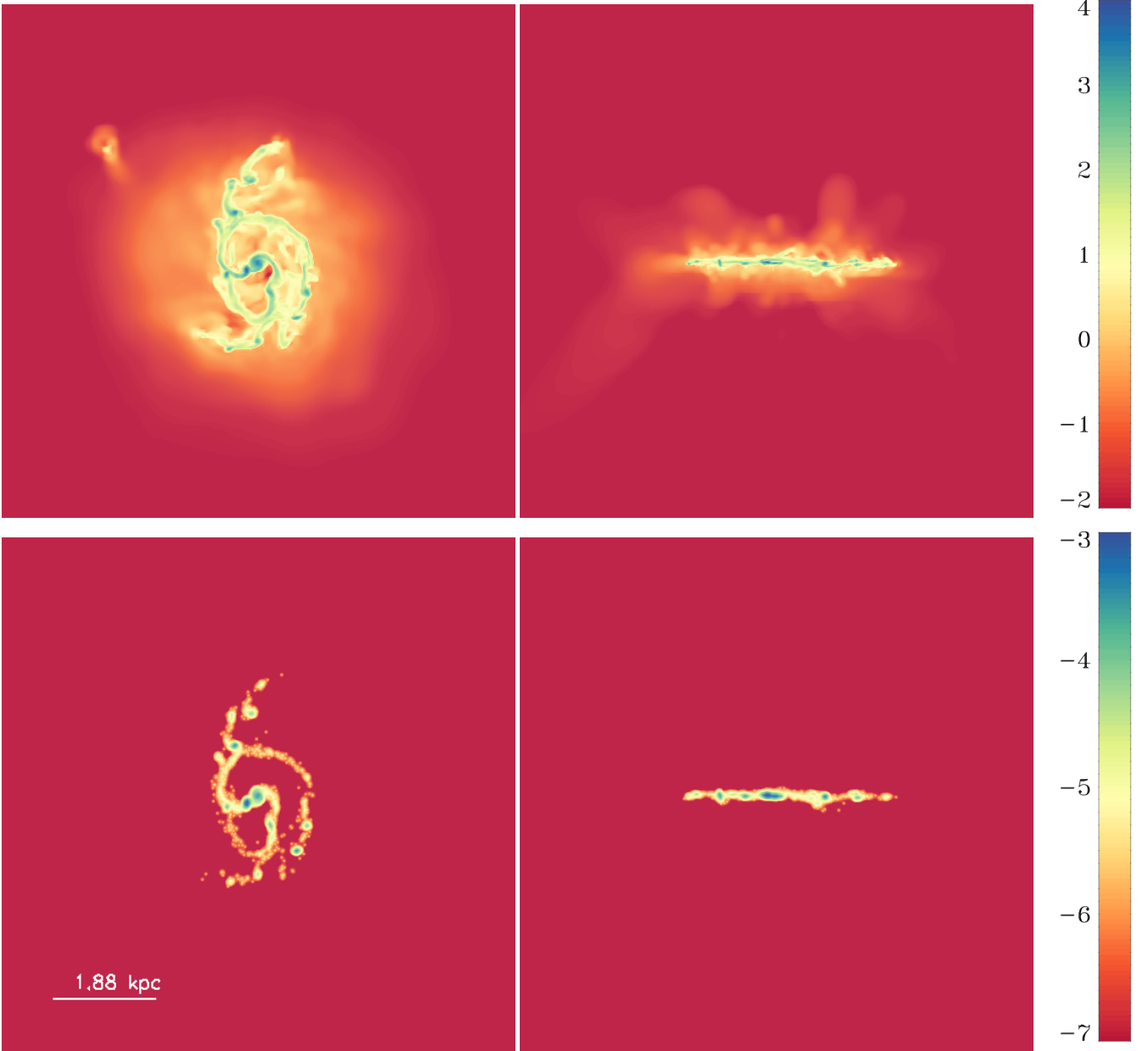


Figure 2. Same as Fig. 1 for the G2 run.

the neutral fraction x is evaluated assuming collisional ionization equilibrium (CIE) and hence only depends on temperature T .

Using the polytropic equation of state (Eq. 1) to prevent artificial fragmentation in the dense ISM unfortunately makes the gas temperature in these regions unknown. In all polytropic cells, we therefore set the temperature of the gas to T_0 ($= 10^4$ K in G1 and 10^2 K in G2). Since we are assuming CIE, these temperatures imply that all the polytropic gas is neutral.

3.2. Velocity dispersion of the gas

The transfer of Ly α photons through a parcel of gas depends on the velocity distribution of the neutral hydrogen atoms in that gas. This dependence appears in the Voigt profile through the Doppler parameter b . In the case of purely thermal motion, $b = v_{\text{th}} = (2k_B T / m_H)^{1/2}$. In the presence of small-scale turbu-

lence, one has to quadratically add the turbulent velocity (v_{turb}) contribution and write $b = (v_{\text{th}}^2 + v_{\text{turb}}^2)^{1/2}$.

In practice, we set $v_{\text{turb}} = 10 \text{ km s}^{-1}$ in both G1 and G2 simulations. This value is the mean value of turbulent velocities computed in simulations of SN-driven turbulence by Dib et al. (2006). We tested the robustness of our results against this assumption by repeating the calculations presented in this paper with $v_{\text{turb}} = 0$ or $v_{\text{turb}} = v_{\text{th}}$. We found no impact on the Ly α escape fractions.

3.3. Dust distribution

In our simulations, gas metallicity is self-consistently calculated from the release of metals in the ISM by SN explosion. The dust distribution is derived from the metallicity distribution by assuming a galactic value for the dust-to-metal (mass) ratio $R_{\text{dust/metal}} = 0.3$ (Inoue 2003). We further assume that dust is

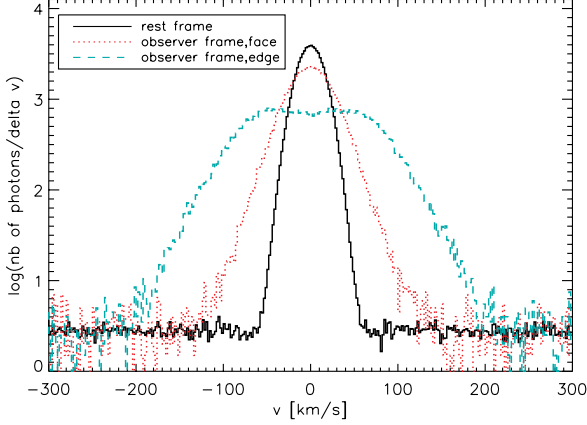


Figure 3. Number of photons emitted per unit velocity bin. The black histogram shows the frequency distribution in the sources frame, as sampled by all photons used in our G2 experiment. This line profile is the one we use as a model for HII regions (Sec. 3.4). The dotted red (resp. dashed blue) histograms show how these photons are distributed in the observer frame when the galaxy is seen face-on (resp. edge-on).

present only in neutral (i.e. $T \lesssim 10^4$ K) media, and write:

$$n_{\text{dust}} = R_{\text{dust/metal}} \frac{Z}{X_{\text{H}}} \frac{m_{\text{H}}}{m_{\text{d}}} n_{\text{HI}}, \quad (3)$$

where Z is the metallicity, $m_{\text{H}}/m_{\text{d}} = 5 \times 10^{-8}$ is the proton to dust particle mass ratio (Draine and Lee 1984), and n_{HI} is the numerical density of *neutral* hydrogen derived in Sec. 3.1.

3.4. The Ly α sources

In the present work, the only mechanism which produces Ly α photons that we take into account is the recombination of photo-ionized gas surrounding massive stars (Kennicutt 1998). In practice, given our resolution, we are effectively using young star particles as a proxy for HII regions and shooting photons from their locations. Note that we only consider star particles younger than 10 Myr as they are the only ones producing significant amounts of ionizing photons (e.g. Charlot and Fall 1993).

Each one of these young star particle emits on average $N_{\text{phot}}/N_{\star}$ photons¹, where N_{phot} is the total number of photons in the experiment, and N_{\star} is the number of young stellar particles in the simulation. In our G1 simulation, we fix $N_{\text{phot}} = 6.4 \cdot 10^5$, and since this simulation has $N_{\star} \sim 10^3$, this implies an average of 640 photons per source. In our G2 simulation, we pick $N_{\text{phot}} \sim 5.1 \cdot 10^6$, and since G2 contains $N_{\star} \sim 3 \cdot 10^4$, this yields an average of 170 photons per source.

In the rest-frame of a star particle, the photons are emitted so as to sample a profile defined by a flat continuum plus a Gaussian line of full-width at half maximum of 20 km s⁻¹, and of equivalent width $\text{EW}(\text{Ly}\alpha) = 200 \text{ \AA}$ (as suggested by e.g. Charlot and Fall 1993; Valls-Gabaud 1993; Schaerer 2003). The continuum extends from -20000 km s⁻¹ to 20000 km s⁻¹ around the Ly α line in the star particle rest-frame, which is way beyond any resonant transfer effect. As an illustration, we show on Fig. 3 the

¹ We deliberately elect not to fix the number of photons per source, but the total number of photons for the whole experiment and sample sources randomly. Thus, the number of photons emitted by each individual star particle has Poissonian variance.

source frame emission profile (black histogram) along with the emitted spectrum (emission from all star particles) of the face-on (red histogram) and edge-on (blue histogram) G2 galaxy in the observer frame.

4. How the ISM structure impacts Ly α transfer

The different temperature floors of the cooling functions used in G1 (10⁴ K) and G2 (100 K) result in strikingly different structures of the ISM. While the gas in G2 is able to fragment into small star-forming clumps, the thermal pressure support in G1 yields a rather smooth ISM with homogeneous star formation. In the present section, we investigate the influence of these structures on the Ly α escape fractions and line profiles.

4.1. Escape fractions

Let us first look at the escape fraction as a function of emission frequency $f_{\text{esc}}(v_{\text{em}})$, defined as the fraction of photons emitted at a frequency v_{em} (in the source rest-frame) which eventually escape the galaxy (i.e. which are not absorbed by dust), whatever their observed frequency. The black curves on Fig. 4 show f_{esc} as a function of v_{em} for G1 (top panel) and G2 (bottom panel).

Before we discuss these curves in more detail, we can partially compare our results to those of Laursen et al. (2009). The simulations of these authors are relatively similar to our G1 simulation in the sense that their cooling curve also stops at 10⁴ K (Sommer-Larsen et al. 2003) and therefore their ISM is unstructured on small scales. As Laursen et al. (2009) only propagate Ly α photons emitted exactly at the Ly α frequency, we have to compare their escape fractions to our value at $v_{\text{em}} = 0$, which is about 55%. This is broadly consistent with their results (their Fig. 9, at $M_{\text{vir}} = 10^{10} M_{\odot}$).

We now turn to the comparison of the escape fractions predicted for G1 and G2 (black curves in Fig. 4). The first remarkable difference is seen in the *continuum* escape fractions², which are $\sim 95\%$ in G1 versus $\sim 22\%$ in G2. This difference has a double origin. The first origin is the very different ISM structures found in G1 and G2. As gas in G2 is able to cool to lower temperatures, it fragments into large star-forming clouds within which most young stellar particles are buried. Instead, gas in G1 has a stronger pressure support and star formation is more diffuse and young stars end up distributed in a rather low density environment. Indeed gas density in G1 does not reach values above 10 atoms per cm³, while gas in G2 reaches 10⁴ atoms per cm³. The second origin is that dust, which we model to scale with the density of metals (and neutral hydrogen) naturally follows star formation. Although it mixes on large scales with time, the dense star-forming clouds of G2 turn out to be more dust-rich than the diffuse (well mixed) ISM of G1. This produces more extinguished young stellar populations in G2, in agreement with e.g. Charlot and Fall (2000).

The second, more subtle point to take from Fig. 4 is that the escape fraction of Ly α photons is also less in G2 than in G1, even when normalized to that of the continuum. Indeed, the ratio of line center to continuum escape fractions in G1 and G2 are respectively $\sim 54\%$ and $\sim 20\%$. We interpret this as a natural effect of resonant scattering of Ly α photons. In the dense clumps of G2 where most photons are emitted, the effect of dust is enhanced by the large H I column densities which increase the path

² Note that the continuum here is only that produced by star particles younger than 10 Myr, and not by the full stellar population of each galaxy.

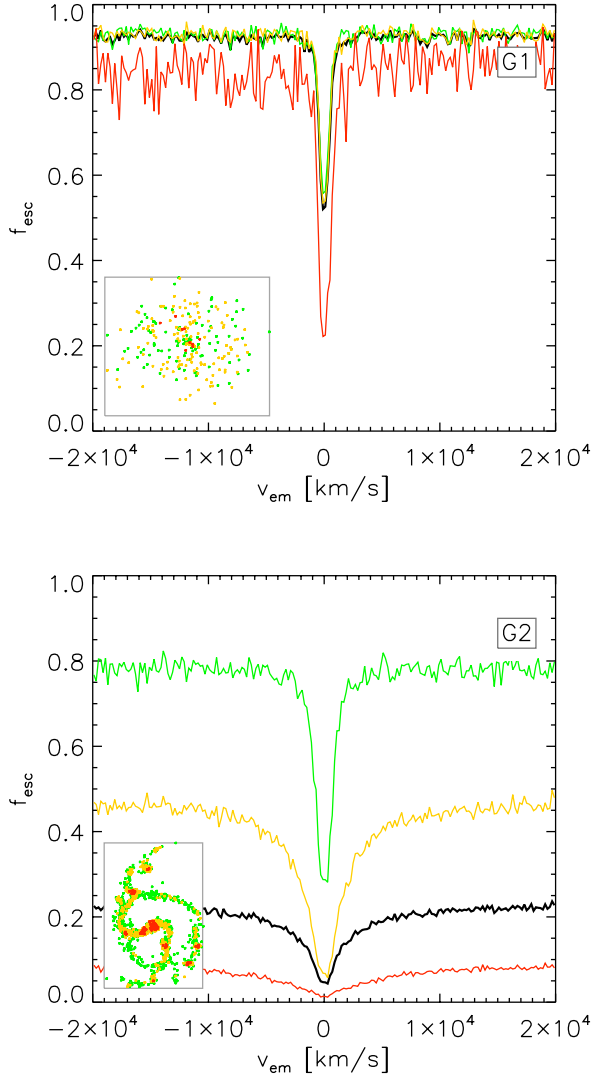


Figure 4. Escape fraction as a function of emitted frequency v_{em} (in the source rest-frame) for simulation G1 (top) and G2 (bottom). The black curves show the spatially integrated escape fractions, i.e. escape fractions averaged over all sources in the galaxy. The red (resp. yellow, green) curves show the escape fractions for sources in the high (resp. average, low) density regions. Thumbnails in the lower-left corner of each panel indicate the face-on position of sources contributing to each of the three curves of the same color.

of photons and hence their likeliness to hit a dust grain. The Ly α escape fractions at the line center vary by an order of magnitude between our two simulated galaxies, from $\sim 50\%$ in G1 to $\sim 5\%$ in G2. Note that our simulations do not include ionising radiation from the stellar sources (or from a UV background). This missing ingredient could increase the escape fractions, and possibly reduce or the difference between G1 and G2. We plan to address this issue in a forthcoming paper.

Fig. 4 also shows color histograms in each panel. These represent the escape fraction distributions for different populations of stars. The red (resp. yellow, green) curves show the escape fractions for photons emitted in high (resp. medium, low) den-

sity environments³. Thumbnail images in the lower left corner of each panel show where the sources contributing to each curve are located in the galaxies (see Figs. 1 and 2 for comparison). The very strong variation of escape fractions with environment in G2, as opposed to the very small variation in G1, is the key to the difference between these two galaxies, and explains our disagreement with the results of Laursen et al. (2009). This different behavior was expected, since the ISM in G1 (along with most simulations in the literature) is artificially smoothed on small scales by the unrealistically large pressure support associated with 10^4 K gas. Hence, the weak radial variation in the escape fraction of G1 simply reflects the gas density gradient in that direction. In G2 however, most young stars lie within very dense and dusty clouds, as expected from e.g. Charlot and Fall (2000), and consequently their Ly α radiation is heavily absorbed. These results demonstrate the necessity to resolve (at least some of) the ISM structure of galaxies with hydrodynamical simulations before post-processing them with Ly α radiative transfer codes in order to make more realistic predictions for the Ly α escape fraction.

It may seem surprising that our results show the opposite trend as that expected in the scenario advocated by Neufeld (1991): we find that a clumpy ISM reduces the escape fraction of Ly α photons relatively to continuum photons instead of enhancing it. The reason for this behavior is that our G2 simulation predicts a configuration which is quite different from that assumed by Neufeld (1991). Whereas this author studies the propagation of photons *through* a clumpy medium, we find that our photons are actually mostly *emitted within the clumps*, and it is their (in)ability to escape from these clumps that dominates the results. Clearly, our G2 simulation still suffers from limitations, both in terms of the simplified assumptions we make to describe the ISM physics (no UV RT but CIE) and in terms of the resolution, which is insufficient to fully resolve HII regions. Bearing these caveats in mind, we find no support for the ‘Neufeld scenario’. We plan to return to this issue with improved simulations in future work.

4.2. Ly α spectra

We now turn to our predicted spectra, i.e. the distribution of *observer-frame* frequencies of photons which escape G1 and G2. We show these spectra in Fig. 5 for three different inclinations: face-on (magenta curves), edge-on (blue curves), and seen from 45 degrees (green curves). Thanks to the symmetry of the problem, we checked that the emergent spectra in all azimuthal directions are the same. The emergent spectra escaping at inclinations $\pm \cos\theta$ are also identical. To increase the statistics, we then sum all photons escaping with $|\cos\theta|$ in the bin corresponding to the chosen inclination, whatever its azimuthal angle ϕ is. The spectra presented on Fig 5 are built by collecting photons within $\cos\theta$ bins large enough to a robust signal, but small enough to keep all the angular variations (e.g. $|\cos\theta| > 0.95$ face-on and $|\cos\theta| < 0.05$ edge-on). Our spectra are *spatially integrated*, i.e. they are emergent spectra along a given direction but from the whole galaxy.

Looking at the spectra emerging from G1 in the top panel of Fig. 5 we see that they are all double-peaked, and roughly symmetrical about the line center. The overall intensity (and the equivalent width) decreases regularly from the face-on to the

³ The cuts in local stellar density that we used vary from G1 to G2, and are defined arbitrarily to capture the different regimes illustrated in Fig. 4.

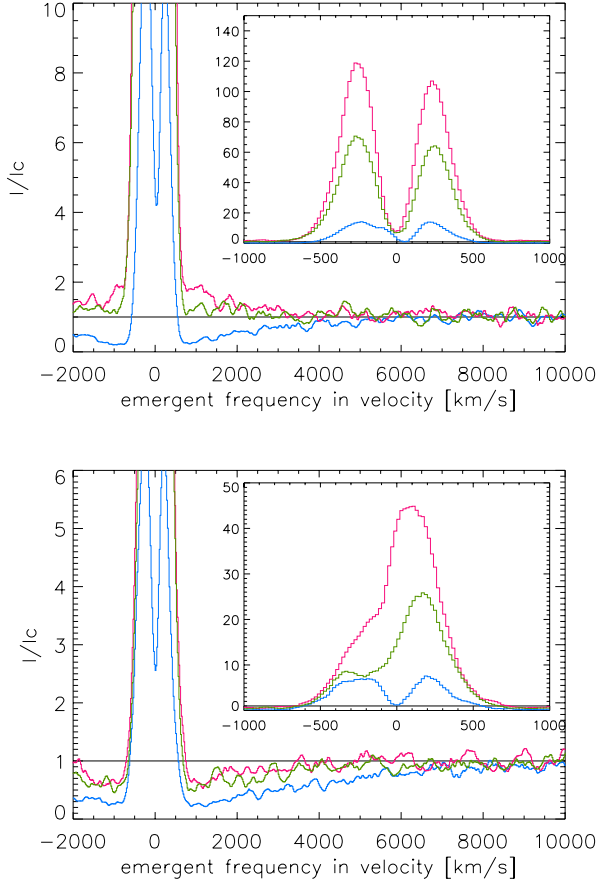


Figure 5. Top : Emergent spectra from G1 along 3 lines of sight ($\theta = 0$ in magenta, $\theta = \pi/4$ in green, $\theta = \pi/2$ in blue). All spectra are *spatially integrated*, i.e. they are emergent spectra along a given direction, but from the whole galaxy. **Bottom :** Same as top panel but for G2.

edge-on view. This is expected since the typical optical depth from the sources to the observer varies in the same way. The double-peaked symmetrical line resembles that expected from transfer through a static homogeneous medium. This is not surprising, since the ISM of G1 is rather homogeneous with a velocity field typical of a globally rotating disk with little internal motions (cf Fig 6, bottom panel). The somewhat higher intensity in the blue peak (at negative velocities) is the result of transfer effects through the gaseous halo, which is in part in-falling towards the galaxy (cf Fig 6, top panel). Indeed, we checked that the spectrum of photons emerging face-on and for which the last scattering is in the halo (above the disk plane) is more asymmetric than that of photons emerging directly from the disk.

The emergent spectrum from G2 (bottom panel of Fig. 5) is also double-peaked edge-on, but clearly asymmetric face-on. The enhancement of the red peak compared to the blue peak is a signature of Ly α diffusing in an outflowing medium, and indeed, gas in G2 is outflowing at much larger velocities (of order a few 100 km/s) than in G1 (where velocities are close to zero or infalling, see Fig 6 and Fig 7, top panels). We checked that if we set the velocity field to 0 km s $^{-1}$ in each cell of the simulation, the spectrum of G2 seen in any direction becomes symmetric about the line center ($v = 0$ km s $^{-1}$). We also reversed the vertical component of the velocity field, v_z , and checked that in this case, the emergent spectrum is reversed, with a more promi-

nent blue peak. Although a very strong large-scale galactic wind is present in G2, this outflowing material is mostly ionized and tenuous, conditions which render it transparent to Ly α photons. As can be seen from Fig. 2 (bottom left panel), SN feedback also pushes cold neutral gas outside the disc, albeit not very far. However, even such a small-scale kinematic feature is enough to produce the asymmetry observed in Fig. 5, because the kinematic energy transferred to this neutral gas is significant (cf Fig 7, top panel).

Even if the asymmetry of the G2 spectra qualitatively compares well to observations (e.g. Kulas et al. 2012, Fig 10), the shift of the peak and the extension of the red tail are less important than in most observed spectra (e.g. Steidel et al. 2010, Fig 1). We attribute (at least part of) this discrepancy to the mass of the galaxy we simulated. This latter is about two orders of magnitude less than typical Lyman-break galaxies, and therefore we can hardly expect its kinematics to have the same amplitude. A wrong implementation of the wind mechanism could cause the same mismatch. The simplified assumptions used to describe the ionisation state of the interstellar gas, i.e. CIE, can also lead to an overestimate of the neutral fraction of the interstellar medium, especially in G2, and affect the spectral shapes. However, investigating different feedback recipes and following UV ionising radiation transfer is beyond the scope of this paper.

5. Orientation effects

We discussed above the impact of the small-scale ISM structure on the propagation and escape of Ly α photons. In the present section, we inspect the global effect of inclination on the observed Ly α properties of our simulated galaxy G2. Indeed, orientation effects were predicted by Charlot and Fall (1993); Chen and Neufeld (1994) and pointed out by recent studies (Laursen and Sommer-Larsen 2007; Laursen et al. 2009; Zheng et al. 2010; Barnes et al. 2011; Yajima et al. 2011b).

5.1. Angular escape fraction and angular redistribution

Let us start by noting that the observed Ly α properties of G2 are, as expected, invariant around the axis of rotation of the disc, i.e. they do not depend on the azimuthal angle. They do however strongly depend on the inclination angle θ , which we define here as the angle from the rotation axis of the disc ($\theta = 0$ face-on and $\theta = \pi/2$ edge-on).

The grey curves in Fig. 8 show the angular escape fractions of continuum (dashed line) and line (solid line) photons⁴. These escape fractions are computed as a function of the inclination at which photons are emitted. The flat solid grey line thus tells us that the escape fraction of line photons is isotropic: whatever direction they are emitted along, only about 5% will escape. On the contrary, continuum photons tend to escape more easily when emitted perpendicular to the disc. Their escape fraction varies from 17% when emitted in the plane to 26% when emitted face-on. The difference between these behaviors is due to resonant scattering. Most line photons scatter a huge number of times (70% scatter more than 10^6 times, less than 10% scatter less than 10 times), enough to forget their initial direction. On the contrary, continuum photons which escape do so without

⁴ We define line photons as having $|v_{\text{em}}| < 100$ km/s in the frame of the sources (see black curve of Fig. 3). For continuum photons, we take photons with $|v_{\text{em}}| > 7000$ km/s.

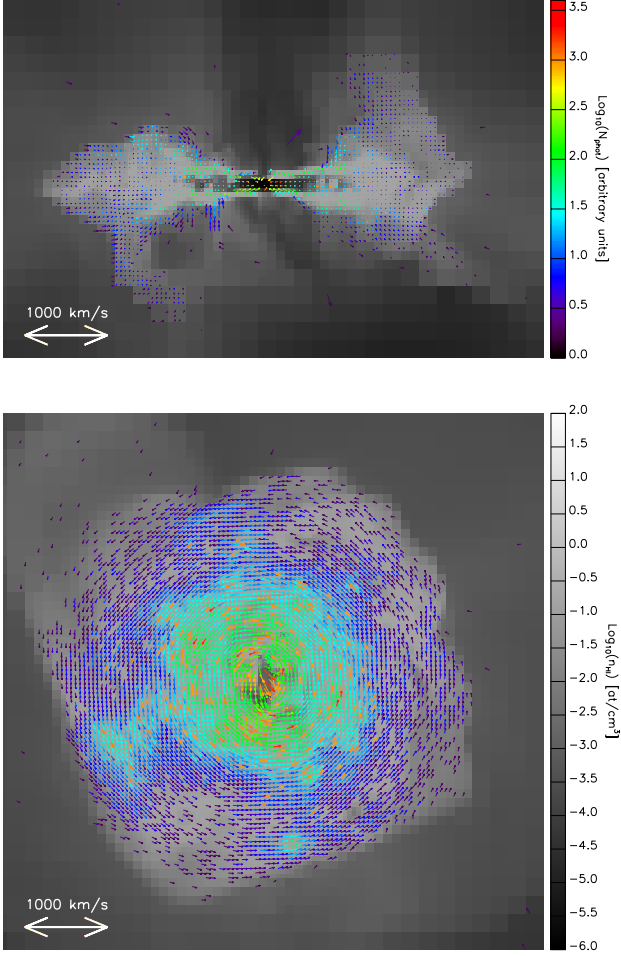


Figure 6. Edge-on (top) and face-on (bottom) views of G1. In both panels, the grey scale indicates the density of neutral Hydrogen (maximum value in a slice of thickness 8 high-resolution cells). The arrows indicate the velocity field of the gas at the location where photons last scatter before they are observed (the double sided arrow in the bottom left corner of each panel gives the scale), and their color scales with the \log_{10} of the number of photons seen from each cell (red: lots of photons, blue: small number of photons).

scattering (about 65% escape directly, and all escape with less than 8 scatterings).

The orange curves in Fig. 8 show the distributions of the inclinations with which the photons escape, i.e. the observed inclination angle distribution, again for continuum (dashed line) and line (solid line) photons. The solid orange curve of Fig. 8 shows a strong angular redistribution of line photons: although they are emitted isotropically and have an isotropic escape fraction, the probability (per unit solid angle) of one escaping face-on is about 15 times higher than that of one escaping edge-on. Similarly, albeit with a much lower amplitude, continuum photons are also redistributed in direction, so that they have a probability 3 times higher to come out face-on than edge-on.

To understand better this angular redistribution, we show in Fig. 9 the relation between observed (y-axis) and emitted (x-axis) inclinations of the photons which escape. The top panel of Fig. 9 shows that indeed, most continuum photons are observed

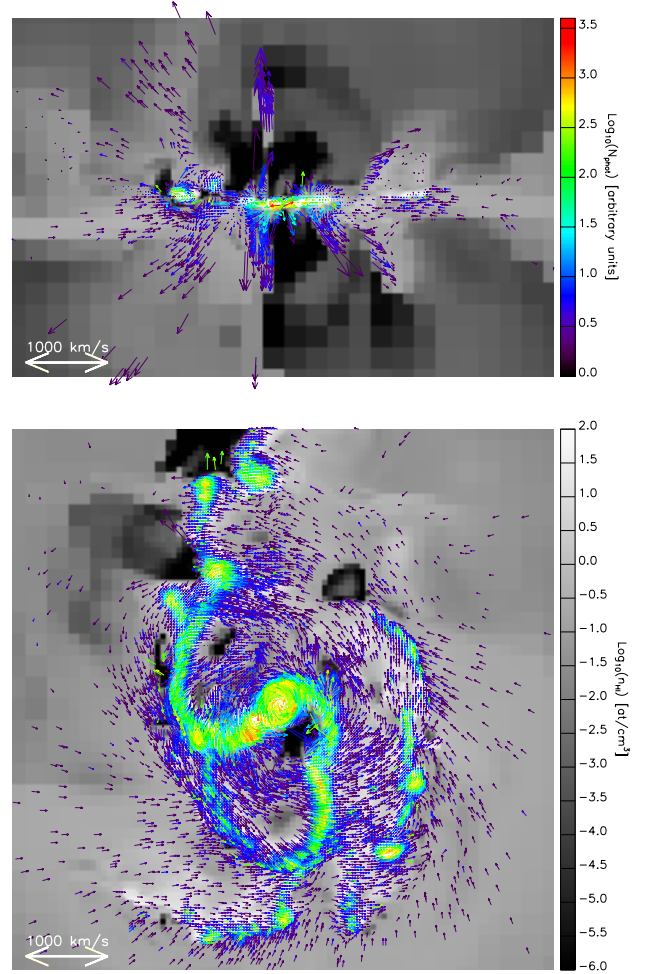


Figure 7. Same as Fig. 6, for G2. Note the much more pronounced vertical motions in the top panel.

with the same inclination as they were emitted with. This panel also shows that a small fraction of continuum photons emitted edge-on are scattered and observed as coming from any direction. The lower panel of Fig. 9 shows that the situation is quite different for line photons. Here, photons only have a marginal chance to escape in the same direction as they were emitted in, provided they were emitted almost face-on, and the overall redistribution is almost independent of the emission inclination. This is due, of course, to the very large number of scatterings that line photons undergo in general.

An early prediction of such orientation effect (favoring face-on escape) was made by Charlot and Fall (1993), by analogy with the stellar 'limb-darkening' effect. However, the enhancement factor that we get (~ 15) is much higher than their prediction (~ 2.3).

This idealised simulation of galaxy formation may be a much more symmetrical configuration than galaxy formation in a cosmological context. However, if still relevant for real galaxies, the strong orientation effect we find has important observational implications. In particular, our results suggest that an LAE survey, which introduces a Ly α luminosity selection, will be biased towards face-on objects, and much more so than e.g. Lyman break surveys which rely on a (UV continuum) broad-band selection. The LAE may hence represent only an incomplete survey of star

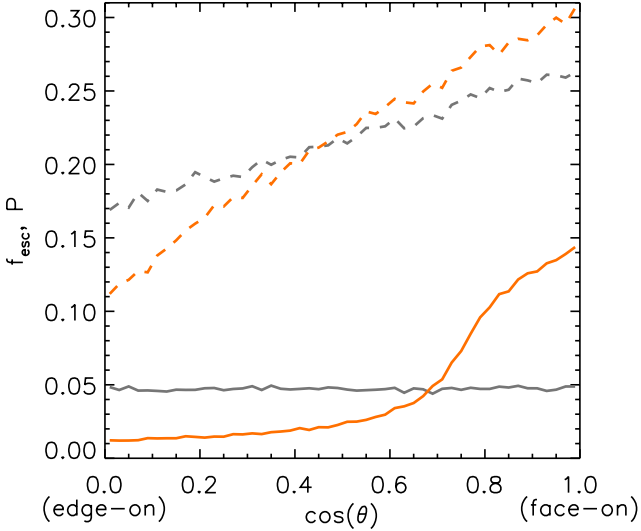


Figure 8. Comparison between the distributions of escape directions in orange, and emission directions in grey, for line (solid lines) and continuum (dashed lines) escaping photons. See the text for a detailed explanation of the shapes of these distributions. Note that the y axis has two different meanings, f_{esc} for the distribution of emission directions, and P for the normalised distribution of escape directions.

forming objects at high redshifts. Also, we expect inclination to introduce a significant scatter in correlations between e.g. SFR and observed Ly α luminosity.

5.2. Ly α equivalent widths

The inclination effect discussed above also manifests itself in the form of a strong correlation between the observed equivalent width and the inclination at which the galaxy is observed. In Fig. 10, we show the EW as a function of the inclination angle, each point corresponding to a random direction of observation. The tight correlation is well fit by a polynomial of the form $EW(\mu) = -8 + 80.7\mu - 393.1\mu^2 + 798.2\mu^3 - 387.4\mu^4$, where $\mu = \cos(\theta)$. This fit is shown with the solid black line. The scatter across the relation is due to variations in the azimuthal angle (ϕ). Note that the EWs we compute here only take into account continuum radiation from stars younger than 10 Myr (the same that are used as sources for Ly α photons), which is good approximation.

The strong dependency of the EW on μ illustrates the differential effect introduced by resonant scattering and discussed with Fig. 8. It shows the complexity of the possible bias introduced by EW selections in narrow-band⁵ LAE samples: not only does the Ly α luminosity of our simulated galaxy strongly vary with inclination, the EW of its emission line does too, and as strongly. For example, with a typical selection at $EW > 20 \text{ \AA}$, our simulated galaxy would be found as a LAE only if observed with an inclination $|\mu| \gtrsim 0.6$, i.e. with $\sim 40\%$ chance assuming a random inclination. In other words, if real galaxies behave similarly to our simulation, LAE narrow-band surveys could be missing $\sim 60\%$ of the faint galaxy population at high redshifts. Even if this number is probably an upper limit, given the symmetry of our idealized galaxy, it calls for observational studies which

⁵ Although narrow band surveys introduce by construction an EW selection, most spectroscopic searches bear such a bias as well.

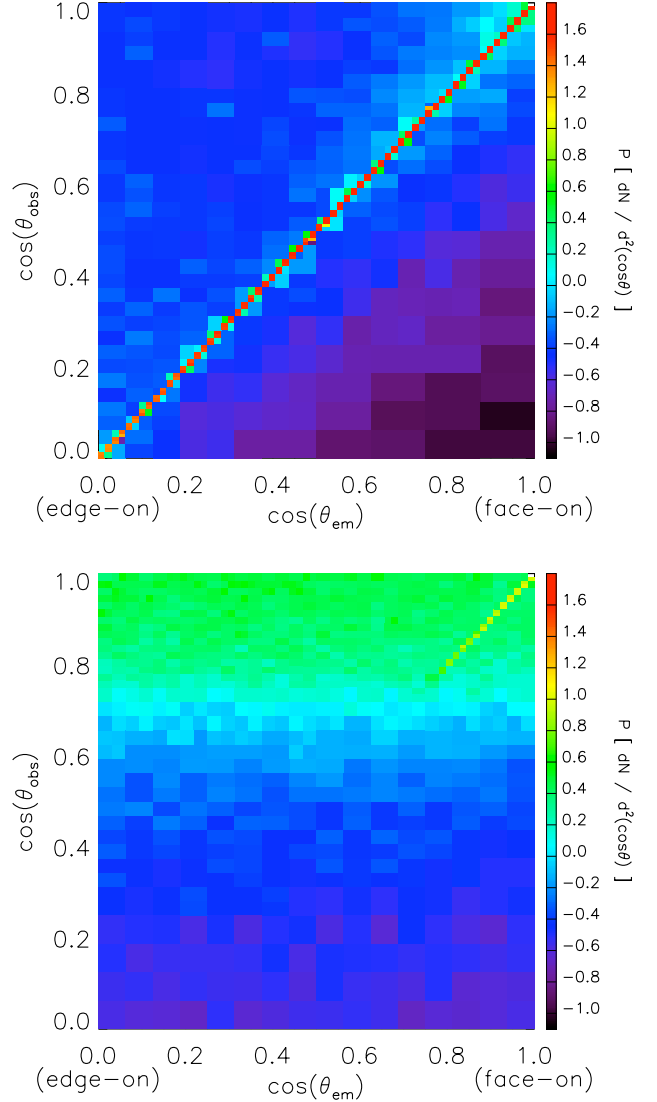


Figure 9. Angular redistribution of continuum (top panel) and line (bottom panel) photons. The x-axis gives the emission direction (as the cosine of the inclination angle), and the y-axis gives the direction along which the photons escape. The color coding scales logarithmically with the number of photon per unit area in the plot, as indicated by the color tables. The white lines on both panels, show the escape fraction as a function of the emission direction.

could assess the effect of inclination on the Ly α properties of real galaxies.

5.3. Line profile

As presented on Fig 5, the emergent spectrum from our realistic ISM model G2 shows a transition in its shape with inclination: the edge-on profile is a double peak symmetrical around the line center, and the face-on spectrum has a much attenuated blue peak. The origin of this behavior is mainly illustrated in Fig. 7 and is as follows. Ly α photons seen escaping edge-on have scattered through an extremely thick medium, with little radial velocities, and the line they produce thus resembles the double peak of a static medium in which photons scatter until

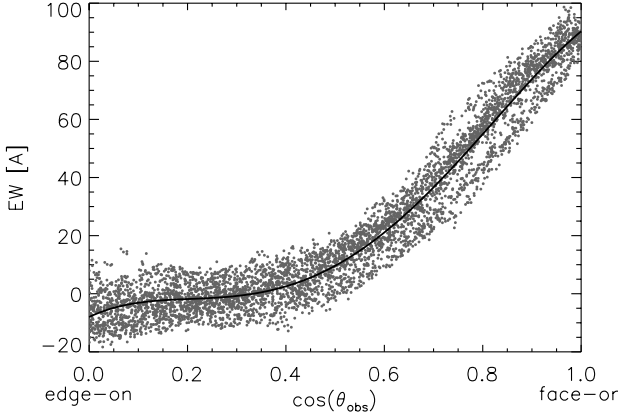


Figure 10. Ly α equivalent widths as a function of the (cosine of the) inclination at which our simulated galaxy is seen. Each point marks one of 5000 mock observations. The solid line is a simple polynomial fit (see text).

they are shifted far enough from the line center to escape. Ly α photons seen face-on, on the contrary, traverse a much lower column density with a much more pronounced velocity field, with gas outflowing at velocities of several 100 km/s, which favors the escape of red-shifted photons.

This evolution of the line profile suggests that the integrated spectral shapes of galaxies may reflect to some extent their inclination, as much as their internal structure and kinematics. Clearly, one would need a larger sample of simulated galaxies to draw robust conclusions here. However, this trend found in our results does hint towards yet another selection effect: Our simulation predicts a correlation between the EW and the line profile, due to the strong correlation that both these quantities have with inclination. This implies that an EW selection will favor asymmetric line profiles and tend to exclude double peaks, which we find to be associated to low inclinations.

6. Ly α halo

On Fig 11, we present face-on (top panel) and edge-on (bottom panel) images⁶ of the galaxy G2 in the Ly α line. Scattering of Ly α photon through the tenuous intra-halo medium produces a diffuse Ly α halo which is clearly visible from both angles. The face-on view only includes photons with $|\cos(\theta)| > 0.95$. The edge-on view includes all photons with escaping $|\cos(\theta)| < 0.2$ so as to have enough statistics, and its surface brightness was renormalized accordingly, so that both panels in Fig.11 are directly comparable. The observed Ly α luminosity face-on is 15% of the intrinsic luminosity (cf Fig 8, $L(\text{Ly}\alpha)_{\text{obs}} = 0.15 \times L(\text{Ly}\alpha)_{\text{int}} \sim 1.8 \times 10^{41} \text{ erg}\cdot\text{s}^{-1}$), whereas it is only a few percent in the edge-on sightline ($\sim 1 - 2 \times 10^{40} \text{ erg}\cdot\text{s}^{-1}$). Such faint galaxy can be observed from $z = 0$ (Östlin et al. 2009, Lyman Alpha Reference Sample.), until $z \sim 3$ (Rauch et al. 2008; Garel et al. 2012). As can be seen from the edge-on view, most of the extended emission comes from scattering on the envelope of the

⁶ Images along a given line of sight described by \mathbf{k}_{los} are obtained by selecting photons escaping in a cone of angle α defined by $-1 < \mathbf{k}_{\text{los}} \cdot \mathbf{k}_{\text{out}} < \cos(\pi - \alpha)$, with α being as small as possible to achieve the best accuracy, and high enough to collect a significant number of photons.

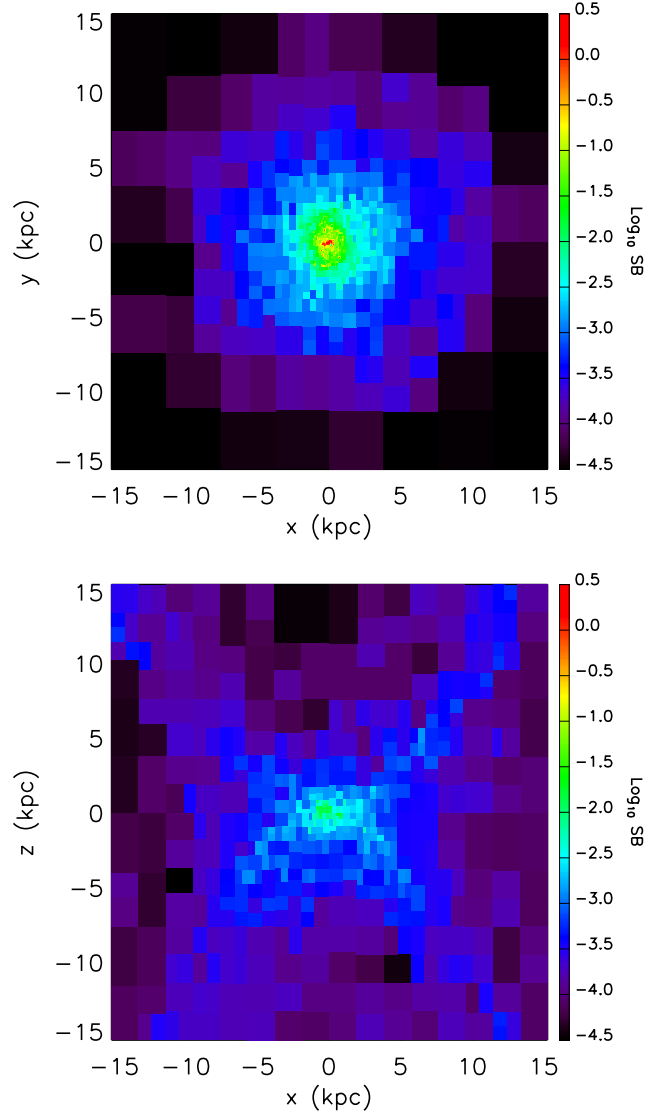


Figure 11. Face-on (top) and edge-on (bottom) views of simulated galaxy G2 in Ly α . The color-coding shows surface brightness in arbitrary units, with the same scale in the two panels.

galactic wind produced by G2, and the hot wind itself is mostly transparent.

This picture is qualitatively comparable to observations by e.g. Hayes et al. (2005); Östlin et al. (2009) or Steidel et al. (2011). Quantitatively, we find that about 40% of Ly α photons come from the central region (within 1.5 kpc), and the rest is diffuse. This does not fit well with the results of Steidel et al. (2011), who find about 5 times more luminosity in the extended halo than in the central region. There are however a number of likely explanations to this apparent disagreement. First, our simulated galaxy is about two orders of magnitude less massive than a typical LBG. Second, and probably more important, our simulation is idealized, and the circum-galactic medium does not feature cold streams or tidal tails which would enhance the effect of scattering. Third, our calculations do not include in-situ emission from cold gas in the halo, either from cooling radiation or UV background fluorescence, and this may play a dominant role here (e.g. Rosdahl and Blaizot 2012).

7. Summary and conclusion

In this paper, we have studied the Ly α properties of a couple of high-resolution simulated dwarf galaxies forming in an idealized dark matter halo. Our two simulations assume different temperature floors of the cooling function (10^4 K for G1, 100K for G2), which result in strikingly different structurations of the ISM. While the gas in G2 is able to fragment into small star-forming clumps, the thermal pressure support in G1 yields a rather smooth ISM with homogeneous star formation. We have post-processed these galaxies with McLy α in order to follow the resonant scattering of Ly α photons through their ISM, and to predict their resultant observational properties. Our main results are as follows.

1. As expected, the small scale structure of the ISM plays a determinant role in shaping a galaxy's Ly α properties. In the G2 simulation, where gas is allowed to cool down to temperatures $\ll 10^4$ K, most young stars are embedded in thick, dusty, star forming clouds, and the photons they emit are strongly attenuated. As opposed to the "Neufeld scenario", the *clumpiness of the ISM here enhances the destruction of Ly α photons relative to continuum photons*. This is due to the fact that photons are emitted within the dense clouds, *à la* Charlot and Fall (2000), rather than outside, as assumed in Neufeld (1991).

In the G1 simulation, with an artificially warm ISM, young stars are found in much lower density environments and their photons escape more easily. This simulation is comparable to the previous studies in the literature which also include dust (Laursen et al. 2009; Yajima et al. 2011a,b), and our results are indeed similar to these studies. Such simulations do not capture the enhancement of Ly α extinction relative to continuum in star-forming regions that we find in G2, simply because they do not form such dense star forming regions.

Another important feature is the kinematic structure of the ISM. Because G2 develops a genuine multiphase medium, with very dense star forming clouds and a tenuous diffuse component, supernovae explosions are able to push gas to high velocities (see Fig. 7). Instead, the rather homogeneous ISM of G1 is overall denser than the diffuse medium of G2, and resists better supernovae explosions. It thus displays a rather static velocity field (see Fig. 6). As shown in Sec. 4.2, these different velocity fields have a strong impact on the shape of Ly α lines.

2. The analysis of Ly α emission from G2⁷ demonstrates the existence of a *strong inclination effect*. Due to the numerous scatterings that line photons undergo, their probability to escape does not depend on the direction towards which they were emitted. Instead, they tend to systematically escape face-on, following the path of least opacity. Because continuum photons do not display such a strong angular redistribution, this effect is directly seen on the Ly α equivalent width, which we find to vary from ~ -5 Å edge-on to ~ 90 Å face-on.

We also find that this inclination effect is seen in the shape of the Ly α line emerging from our simulated galaxy. When seen edge-on, our galaxy has a double-peak line, associated with a low EW. When seen face-on, our galaxy has an enhanced red peak, and a high EW.

These results suggest the possible existence of strong observational biases in LAE surveys which necessarily rely on Ly α luminosity and EW selections, and could thus prefer-

entially select face-on objects. As an example, a survey with an EW cut at 20 Å would select our galaxy only 40% of the times, assuming it has a random inclination.

3. Scattering of galactic Ly α photons through the circumgalactic medium do produce an extended Ly α halo. We find that about a third of Ly α photons escaping G2 contribute to this diffuse component. This is somewhat at odds with the results of Steidel et al. (2011), though the comparison should be taken with caution given the fact that our simulated galaxy has a much smaller mass than the galaxies analyzed by these authors. Also, our simulation is idealized, and the CGM of G2 is not a good representation of what one finds in cosmological simulations at high redshift (Rosdahl and Blaizot 2012; Dubois et al. 2012).

Although our quantitative results are clearly limited by much missing physics, we believe that this work demonstrates the two main following points: (1) resolving the ISM is mandatory if we want to understand the escape fraction of Ly α from galaxies (it doesn't matter here if we have the correct solution: we show how widely the results vary when we change the ISM physics ... and this definitely shows that we should go further); and (2) for an ideal disc galaxy, we find that the escape fraction is a strong function of inclination, and we argue that this effect is quite possibly present in real galaxies (eventhough their morphologies are known to be more complex). Both results call for more work, both theoretically and observationally. From the theoretical viewpoint, we plan to make progress in forthcoming papers by (i) including the transfer of ionizing photons through a *resolved* ISM, and (ii) embedding our galaxy in the full complexity of its cosmological context.

Acknowledgements. AV was supported by a Fellowship for prospective researchers of the Swiss National Science Foundation to start this project in Oxford, and by a Marie Curie Intra European Fellowship within the 7th European Community Framework Programme in Lyon. YD is supported by an STFC Postdoctoral Fellowship. The simulations presented here were run on the TITANE cluster at the Centre de Calcul Recherche et Technologie of CEA Saclay on allocated resources from the GENCI grant c2009046197. JB acknowledges support from the ANR BINGO project (ANR-08-BLAN-0316-01).

References

- L. A. Barnes, M. G. Haehnelt, E. Tescari, and M. Viel. Galactic winds and extended Ly α emission from the host galaxies of high column density quasar absorption systems. *MNRAS*, 416:1723–1738, September 2011.
- R. M. Bielby, T. Shanks, P. M. Weibacher, L. Infante, N. H. M. Crighton, C. Bornancini, N. Bouché, P. Héraudeau, D. G. Lambas, J. Lowenthal, D. Minniti, N. Padilla, P. Petitjean, and T. Theuns. The VLT LBG Redshift Survey - I. Clustering and dynamics of ~ 1000 galaxies at $z \sim 3$. *MNRAS*, 414:2–27, June 2011.
- J. S. Bullock, A. Dekel, T. S. Kolatt, A. V. Kravtsov, A. A. Klypin, C. Porciani, and J. R. Primack. A Universal Angular Momentum Profile for Galactic Halos. *ApJ*, 555:240–257, July 2001.
- P. Cassata, O. Le Fèvre, B. Garilli, D. Maccagni, V. Le Brun, M. Scodeggio, L. Tresse, O. Ilbert, G. Zamorani, O. Cucciati, T. Contini, R. Bielby, Y. Mellier, H. J. McCracken, A. Pollo, A. Zanichelli, S. Bardelli, A. Cappi, L. Pozzetti, D. Vergani, and E. Zucca. The VIMOS VLT Deep Survey: star formation rate density of Ly α emitters from a sample of 217 galaxies with spectroscopic redshifts $2 < z < 6.6$. *A&A*, 525:A143, January 2011.
- S. Charlot and S. M. Fall. Lyman-Alpha Emission from Galaxies. *ApJ*, 415:580–+, October 1993.
- S. Charlot and S. M. Fall. A Simple Model for the Absorption of Starlight by Dust in Galaxies. *ApJ*, 539:718–731, August 2000.
- W. L. Chen and D. A. Neufeld. Ly(alpha) emission and absorption features in the spectra of galaxies. *ApJ*, 432:567–574, September 1994.
- P. Dayal, A. Ferrara, and S. Gallerani. Signatures of reionization on Ly α emitters. *MNRAS*, 389:1683–1696, October 2008.
- P. Dayal, A. Ferrara, A. Saro, R. Salvaterra, S. Borgani, and L. Tornatore. Lyman alpha emitter evolution in the reionization epoch. *MNRAS*, 400:2000–2011, December 2009.

⁷ and G1, although we do not show it here

- P. Dayal, A. Maselli, and A. Ferrara. The visibility of Lyman α emitters during reionization. *MNRAS*, 410:830–843, January 2011. .
- S. Dib, E. Bell, and A. Burkert. The Supernova Rate-Velocity Dispersion Relation in the Interstellar Medium. *ApJ*, 638:797–810, February 2006. .
- M. Dijkstra and A. Loeb. The polarization of scattered Ly α radiation around high-redshift galaxies. *MNRAS*, 386:492–504, May 2008. .
- M. Dijkstra, Z. Haiman, and M. Spaans. Ly α Radiation from Collapsing Protogalaxies. I. Characteristics of the Emergent Spectrum. *ApJ*, 649:14–36, September 2006. .
- B. T. Draine and H. M. Lee. Optical properties of interstellar graphite and silicate grains. *ApJ*, 285:89–108, October 1984. .
- Y. Dubois and R. Teyssier. On the onset of galactic winds in quiescent star forming galaxies. *A&A*, 477:79–94, January 2008. .
- Y. Dubois, C. Pichon, M. Haehnelt, T. Kimm, A. Slyz, J. Devriendt, and D. Pogosyan. Feeding compact bulges and supermassive black holes with low angular momentum cosmic gas at high redshift. *MNRAS*, page 3123, May 2012. .
- T. Garel, J. Blaizot, B. Guiderdoni, D. Schaerer, A. Verhamme, and M. Hayes. Modelling high redshift Lyman α emitters. *MNRAS*, 422:310–325, May 2012. .
- M. Hayes, G. Östlin, J. M. Mas-Hesse, D. Kunth, C. Leitherer, and A. Petrosian. HST/ACS Lyman α imaging of the nearby starburst ESO 338-IG04. *A&A*, 438:71–85, July 2005. .
- E. M. Hu, L. L. Cowie, and R. G. McMahon. The Density of Ly alpha Emitters at Very High Redshift. *ApJL*, 502:L99, August 1998. .
- E. M. Hu, L. L. Cowie, A. J. Barger, P. Capak, Y. Kakazu, and L. Trouille. An Atlas of $z = 5.7$ and $z = 6.5$ Ly α Emitters. *ApJ*, 725:394–423, December 2010. .
- A. K. Inoue. Evolution of Dust-to-Metal Ratio in Galaxies. *PASJ*, 55:901–909, October 2003. .
- R. C. Kennicutt, Jr. The Global Schmidt Law in Star-forming Galaxies. *ApJ*, 498:541, May 1998. .
- E. Komatsu, K. M. Smith, J. Dunkley, C. L. Bennett, B. Gold, G. Hinshaw, N. Jarosik, D. Larson, M. R. Nolta, L. Page, D. N. Spergel, M. Halpern, R. S. Hill, A. Kogut, M. Limon, S. S. Meyer, N. Odegard, G. S. Tucker, J. L. Weiland, E. Wollack, and E. L. Wright. Seven-year Wilkinson Microwave Anisotropy Probe (WMAP) Observations: Cosmological Interpretation. *ApJS*, 192:18, February 2011. .
- A. V. Kravtsov and O. Y. Gnedin. Formation of Globular Clusters in Hierarchical Cosmology. *ApJ*, 623:650–665, April 2005. .
- M. R. Krumholz and J. C. Tan. Slow Star Formation in Dense Gas: Evidence and Implications. *ApJ*, 654:304–315, January 2007. .
- R.-P. Kudritzki, R. H. Méndez, J. J. Feldmeier, R. Ciardullo, G. H. Jacoby, K. C. Freeman, M. Arnaboldi, M. Capaccioli, O. Gerhard, and H. C. Ford. Discovery of Nine Ly α Emitters at Redshift $z \sim 3.1$ Using Narrowband Imaging and VLT Spectroscopy. *ApJ*, 536:19–30, June 2000. .
- K. R. Kulas, A. E. Shapley, J. A. Kollmeier, Z. Zheng, C. C. Steidel, and K. N. Hainline. The Kinematics of Multiple-peaked Ly α Emission in Star-forming Galaxies at $z \sim 2.3$. *ApJ*, 745:33, January 2012. .
- P. Laursen and J. Sommer-Larsen. Ly α Resonant Scattering in Young Galaxies: Predictions from Cosmological Simulations. *ApJL*, 657:L69–L72, March 2007. .
- P. Laursen, J. Sommer-Larsen, and A. C. Andersen. Ly α Radiative Transfer with Dust: Escape Fractions from Simulated High-Redshift Galaxies. *ApJ*, 704:1640–1656, October 2009. .
- M. Le Delliou, C. G. Lacey, C. M. Baugh, and S. L. Morris. The properties of Ly α emitting galaxies in hierarchical galaxy formation models. *MNRAS*, 365:712–726, January 2006. .
- J. F. Navarro and S. D. M. White. Simulations of Dissipative Galaxy Formation in Hierarchically Clustering Universes - Part One - Tests of the Code. *MNRAS*, 265:271–+, November 1993. .
- J. F. Navarro, C. S. Frenk, and S. D. M. White. The Structure of Cold Dark Matter Halos. *ApJ*, 462:563–+, May 1996. .
- D. A. Neufeld. The escape of Lyman-alpha radiation from a multiphase interstellar medium. *ApJL*, 370:L85–L88, April 1991. .
- A. Orsi, C. G. Lacey, C. M. Baugh, and L. Infante. The clustering of Ly α emitters in a Λ CDM Universe. *MNRAS*, 391:1589–1604, December 2008. .
- A. Orsi, C. G. Lacey, and C. M. Baugh. Can galactic outflows explain the properties of Ly-alpha emitters? *ArXiv e-prints*, October 2011. .
- G. Östlin, M. Hayes, D. Kunth, J. M. Mas-Hesse, C. Leitherer, A. Petrosian, and H. Atek. The Lyman Alpha Morphology of Local Starburst Galaxies: Release of Calibrated Images. *AJ*, 138:923–940, September 2009. .
- M. Ouchi, K. Shimasaku, M. Akiyama, C. Simpson, T. Saito, Y. Ueda, H. Furusawa, K. Sekiguchi, T. Yamada, T. Kodama, N. Kashikawa, S. Okamura, M. Iye, T. Takata, M. Yoshida, and M. Yoshida. The Subaru/XMM-Newton Deep Survey (SXDS). IV. Evolution of Ly α Emitters from $z=3.1$ to 5.7 in the 1 deg^2 Field: Luminosity Functions and AGN. *ApJS*, 176:301–330, June 2008. .
- M. Ouchi, K. Shimasaku, H. Furusawa, T. Saito, M. Yoshida, M. Akiyama, Y. Ono, T. Yamada, K. Ota, N. Kashikawa, M. Iye, T. Kodama, S. Okamura, C. Simpson, and M. Yoshida. Statistics of 207 Ly α Emitters at a Redshift Near 7: Constraints on Reionization and Galaxy Formation Models. *ApJ*, 723:869–894, November 2010. .
- Y. Rasera and R. Teyssier. The history of the baryon budget. Cosmic logistics in a hierarchical universe. *A&A*, 445:1–27, January 2006. .
- M. Rauch, M. Haehnelt, A. Bunker, G. Becker, F. Marleau, J. Graham, S. Cristiani, M. Jarvis, C. Lacey, S. Morris, C. Peroux, H. Röttgering, and T. Theuns. A Population of Faint Extended Line Emitters and the Host Galaxies of Optically Thick QSO Absorption Systems. *ApJ*, 681:856–880, July 2008. .
- J. Rosdahl and J. Blaizot. Extended Ly α emission from cold accretion streams. *MNRAS*, page 2837, April 2012. .
- A. Rosen and J. N. Bregman. Global Models of the Interstellar Medium in Disk Galaxies. *ApJ*, 440:634, February 1995. .
- E. E. Salpeter. The Luminosity Function and Stellar Evolution. *ApJ*, 121:161–+, January 1955. .
- D. Schaerer. The transition from Population III to normal galaxies: Ly α and He II emission and the ionising properties of high redshift starburst galaxies. *A&A*, 397:527–538, January 2003. .
- D. Schaerer, M. Hayes, A. Verhamme, and R. Teyssier. Grid of Ly α radiation transfer models for interpreting distant galaxies. *A&A*, 531:A12+, July 2011. .
- A. E. Shapley, C. C. Steidel, M. Pettini, and K. L. Adelberger. Rest-Frame Ultraviolet Spectra of $z \sim 3$ Lyman Break Galaxies. *ApJ*, 588:65–89, May 2003. .
- K. Shimasaku, N. Kashikawa, M. Doi, C. Ly, M. A. Malkan, Y. Matsuda, M. Ouchi, T. Hayashino, M. Iye, K. Motohara, T. Murayama, T. Nagao, K. Ohta, S. Okamura, T. Sasaki, Y. Shioya, and Y. Taniguchi. Ly α Emitters at $z = 5.7$ in the Subaru Deep Field. *PASJ*, 58:313–334, April 2006. .
- J. Sommer-Larsen. Where Are the “Missing” Galactic Baryons? *ApJL*, 644:L1–L4, June 2006. .
- J. Sommer-Larsen, M. Götz, and L. Portinari. Galaxy Formation: Cold Dark Matter, Feedback, and the Hubble Sequence. *ApJ*, 596:47–66, October 2003. .
- C. C. Steidel, D. K. Erb, A. E. Shapley, M. Pettini, N. Reddy, M. Bogosavljević, G. C. Rudie, and O. Rakic. The Structure and Kinematics of the Circumgalactic Medium from Far-ultraviolet Spectra of $z \sim 2-3$ Galaxies. *ApJ*, 717:289–322, July 2010. .
- C. C. Steidel, M. Bogosavljević, A. E. Shapley, J. A. Kollmeier, N. A. Reddy, D. K. Erb, and M. Pettini. Diffuse Ly α Emitting Halos: A Generic Property of High-redshift Star-forming Galaxies. *ApJ*, 736:160, August 2011. .
- J. O. Stenflo. Resonance-line polarization. V - Quantum-mechanical interference between states of different total angular momentum. *A&A*, 84:68–74, April 1980. .
- R. S. Sutherland and M. A. Dopita. Cooling functions for low-density astrophysical plasmas. *ApJS*, 88:253–327, September 1993. .
- C. Tapken, I. Appenzeller, S. Noll, S. Richling, J. Heidt, E. Meinköhn, and D. Mehlert. Ly α emission in high-redshift galaxies. *A&A*, 467:63–72, May 2007. .
- A. Tasitsiomi. Ly α Radiative Transfer in Cosmological Simulations and Application to a $z \sim 8$ Ly α Emitter. *ApJ*, 645:792–813, July 2006. .
- E. Tescari, M. Viel, L. Tornatore, and S. Borgani. Damped Lyman α systems in high-resolution hydrodynamical simulations. *MNRAS*, 397:411–430, July 2009. .
- R. Teyssier. Cosmological hydrodynamics with adaptive mesh refinement. A new high resolution code called RAMSES. *A&A*, 385:337–364, April 2002. .
- J. K. Truelove, R. I. Klein, C. F. McKee, J. H. Holliman, II, L. H. Howell, and J. A. Greenough. The Jeans Condition: A New Constraint on Spatial Resolution in Simulations of Isothermal Self-gravitational Hydrodynamics. *ApJL*, 489:L179+, November 1997. .
- D. Valls-Gabaud. On the Lyman-Alpha Emission of Starburst Galaxies. *ApJ*, 419:7–+, December 1993. .
- C. van Breukelen, M. J. Jarvis, and B. P. Venemans. The luminosity function of Ly α emitters at $2.3 < z < 4.6$ from integral-field spectroscopy*. *MNRAS*, 359:895–905, May 2005. .
- A. Verhamme, D. Schaerer, and A. Maselli. 3D Ly α radiation transfer. I. Understanding Ly α line profile morphologies. *A&A*, 460:397–413, December 2006. .
- A. N. Witt and K. D. Gordon. Multiple Scattering in Clumpy Media. II. Galactic Environments. *ApJ*, 528:799–816, January 2000. .
- H. Yajima, Y. Li, Q. Zhu, and T. Abel. ART²: Coupling Lyman-alpha Line and Multi-wavelength Continuum Radiative Transfer. *ArXiv e-prints*, September 2011a. .
- H. Yajima, Y. Li, Q. Zhu, T. Abel, C. Gronwall, and R. Ciardullo. Were progenitors of local L* galaxies Lyman-alpha emitters at high redshift? *ArXiv*

e-prints, December 2011b.

- Z. Zheng and J. Miralda-Escudé. Monte Carlo Simulation of Ly α Scattering and Application to Damped Ly α Systems. *ApJ*, 578:33–42, October 2002. .
- Z. Zheng, R. Cen, H. Trac, and J. Miralda-Escudé. Radiative Transfer Modeling of Ly α Emitters. I. Statistics of Spectra and Luminosity. *ApJ*, 716:574–598, June 2010. .